mater.scichina.com link.springer.com Published online 18 February 2022 | https://doi.org/10.1007/s40843-021-1940-2

Biomimetic brain-like nanostructures for solid polymer electrolytes with fast ion transport

Ahmed Eissa Abdelmaoula[1,3†], Lulu Du[1†], Lin Xu[1,2*], Yu Cheng[1], Amir A. Mahdy[3], Muhammad Tahir[1], Ziang Liu[1] and Liqiang Mai[1,2*]

ABSTRACT **The intrinsic drawbacks of electrolytes and the growth of lithium dendrites limit the development of commercial lithium batteries. To address the aforementioned challenges, a novel biomimetic brain-like nanostructure (BBLN) solid polymer electrolyte was created by manipulating the shape of the incorporated nanoparticles. Our designed BBLN solid polymer electrolyte was created by incorporating spherical core-shell (UIO-66@67) fillers into polymer electrolyte, which is significantly different from traditional polymer-based composite electrolytes. UIO-66@67 spherical nanoparticles are highly favorable to eliminating polymer electrolyte stress and deformation during solidification, indicating a great potential for fabricating highly uniform BBLN solid polymer electrolytes with a substantial number of continuous convolutions. Furthermore, spherical nanoparticles can significantly reduce the crystalline structure of polymer electrolytes, improving polymer chain segmental movement and providing continuous pathways for rapid ion transfer. As a result, BBLN solid polymer electrolyte shows excellent ionic conductivity (9.2×10^{-4} S cm^{-1}), a high lithium transference number (0.74), and outstanding cycle stability against lithium electrodes over 6500 h at room temperature. The concept of biomimetic brain-like nanostructures in this work demonstrates a novel strategy to enhance ion transport in polymer-based electrolytes for solid-state batteries.**

Keywords: brain structure, spherical nanoparticles, continuous interphase, nanophase separation, MOF-in-MOF

INTRODUCTION

With the dramatic increases in electric vehicles and portable electronic devices, traditional lithium-ion batteries (LIBs) with organic liquid electrolytes are facing difficulties in terms of safety concerns and energy density [1–7]. Solid-state LIBs based on solid electrolytes have received increased attention as potential next-generation rechargeable batteries capable of significantly overcoming the limitations of traditional LIBs [8–14]. Furthermore, solid electrolytes based on polymer or hybrid solid electrolytes are considered ideal choices for LIBs due to their wide voltage windows, easy fabrication, and excellent flexibility [15–22]. Various approaches have used metal-organic frameworks (MOFs) as a solid electrolyte in LIBs to enhance the transport of Li^+, strengthen the mechanical properties, and improve the electrochemical stability against electrodes [23–27]. Moreover, developing solid-state electrolytes with low interfacial resistance, high ionic conductivity, and the ability to suppress the formation of lithium dendrites is highly desirable and continues to be a significant challenge.

Interwoven and intercommunicating structures play an important role in many scientific fields like materials science, medicine, and information technology due to their versatile functionality. Brain-like nanostructures are being extensively researched as an intriguing class of interconnected systems for improving mass and information transport. The brain is an extraordinarily complex system of interlaced, intercommunicating cells with diameters ranging from 5 to 50 μm; brain tissues function as porous channels for nutrient and drug transport. Diffusion is the main delivery mechanism in the brain: aside from transporting oxygen and glucose from the vasculature to brain cells, it further transports the information between cells [28,29]. Several studies, on the other hand, have shown that the brain structure is the best way to deliver informational substances and mass between various components [30–36].

The mixing of different materials is one of the most common methods for creating such structures. The shape and physical properties of the incorporated particles generally affect the morphology and deformation degree of the component during solidification, consequently affecting the properties of the new material [37]. Zhu *et al.* [38] used an aniline/citric acid salt template and chlorine gas as the oxidant in a gas/solid reaction to prepare a brain-like polyaniline nanostructure with numerous convolutions and diameters ranging from 140 to 170 nm. Seo *et al.* [39] successfully synthesized "brain-coral-like" materials based on ZIF chemistry, with high sulfur loading, excellent cyclic stability, and efficient lithium polysulfides adsorption. To the best of our knowledge, no study has designed and fabricated the brain-like nanostructure by adding spherical nanoparticles. Our group investigated the possibility of creating an electrolyte

[1] State Key Laboratory of Advanced Technology for Materials Synthesis and Processing, School of Materials Science and Engineering, Wuhan University of Technology, Wuhan 430070, China
[2] Foshan Xianhu Laboratory of the Advanced Energy Science and Technology Guangdong Laboratory, Xianhu Hydrogen Valley, Foshan 528200, China
[3] Mining and Metallurgical Department, Faculty of Engineering, Al-Azhar University, Cairo 11884, Egypt
† These authors contributed equally to this paper.
* Corresponding authors (emails: linxu@whut.edu.cn (Xu L); mlq518@whut.edu.cn (Mai L))

with a brain-like nanostructure by controlling the shape of the embedded nanoparticles to mimic the above properties of brain structure.

In this work, inspired by the brain structure, we propose biomimetic brain-like nanostructures (BBLN) for solid polymer electrolytes with fast ion transport. By incorporating MOF-in-MOF spherical nanoparticles into polyethleneoxide-lithium bis-trifluoromethanesulfonimide (PEO-LiTFSI), highly uniform BBLN solid polymer electrolyte was created. Spherical nanoparticles with smooth edges are highly appealing for reducing stress and deformation in polymer electrolytes during solidification, indicating a high potential for fabricating highly uniform BBLN solid polymer electrolytes. Besides, spherical nanoparticles not only increase the surface area of the polymer by transferring it to a continuous brain-like nanostructure, but they also produce nanostructured phase separation, which significantly reduces the crystallinity of polymer electrolytes. Moreover, the larger surface area of spherical nanoparticles compared with other shapes improves the contact area with polymer, increasing the strength of polymer electrolytes. Finally, the surface morphology of BBLN has a significant impact on electrolyte performance, indicating that the rough surface improves lithium-ion transport by increasing the effective contact area between the electrolyte and electrodes. Based on the above, the as-prepared BBLN polymer electrolyte showed a superb electrochemical property such as an excellent ionic conductivity of 9.2×10^{-4} S cm^{-1} at room temperature, and high lithium transference number (t_{Li^+}) of 0.74. In addition, the assembled LIBs based on the BBLN solid polymer electrolyte demonstrated an excellent capacity of 155 mA h g^{-1} for 200 cycles at 25°C.

EXPERIMENTAL SECTION

Synthetic procedures

Biphenydicarboxylic acid (99%) and 1,4-benzenedicarboxylic acid (99%) were purchased from Macklin. Zirconium (IV) chloride (98%), 1-ethyl-3-methylimidazolium bis(trifluoromethylsulfonyl)imide (EMIM-TFSI, 97%), LiTFSI (97%), glacial acetic acid (99.7%), benzoic acid (99%), hydrochloric acid (36%–38%), and *N*,*N*-dimethyl formamide (DMF, 99%) were purchased from Aladdin. All of the reactants and solvents were analytical grade and used without further purification.

UIO-66 was prepared based on the previous report [40]. Briefly, $ZrCl_4$ (340 mg) and DMF (40 mL) were mixed in a Teflon-lined autoclave by sonication for about 15 min. Terephthalic acid and acetic acid were combined, and then sonicated for 15 min until completely dissolved. The autoclave was placed in an oven at 120°C for 24 h. After cooling, the nanocrystalline MOF was collected by centrifuging at 10,000 r min^{-1} for 8 min, and washed three times sequentially by DMF (3 × 30 mL) and EtOH (3 × 30 mL) before being dried in vacuum at 60°C.

UIO-67 was prepared based on the reported method [41]. Briefly, 502 mg of $ZrCl_4$, 2.63 g of benzoic acid, and 520 mg of nitroterephthalic acid (H_2BPDC) were dissolved under sonication in a mixing solution (50 mL DMF with 0.152 mL HCl) for 20 min. The homogeneous mixture was transferred at room temperature to a Teflon-lined hydrothermal autoclave before being heated at 130°C for 48 h. After cooling in air to room temperature, the resulting white precipitate was centrifuged at 1000 r min^{-1} for 8 min and repeatedly washed and dried using the same procedure as UIO-66.

UIO-66@67 core-shell nanoparticles were fabricated by a solvothermal method with two linkers. Briefly, 140 mg of UIO-66 nanoparticles, 93.2 mg of $ZrCl_4$, 97.6 mg of H_2BPDC, 488 mg of benzoic acid, 0.8 mL of glacial acetic, and 50 mL of DMF were sonicated for 30 min in a Teflon-lined hydrothermal autoclave to achieve a homogeneous mixture before being heated at 130°C for 36 h. The precipitate was collected by centrifuging at 10,000 r min^{-1} for 8 min, and then washed repeatedly with the same procedure as UIO-66, and the obtained MOF was activated at 200°C for 1 h at a heating rate of 1°C/2 min.

Preparation of Li-ionic liquid (IL)/MOF: LiTFSI (0.6975 g) and EMIM-TFSI (2.5 mL) were mixed using a magnetic stirrer for 1 h at room temperature before heating at 120°C/12 h to obtain Li-IL. The activated UIO-66@67, UIO-66, and UIO-67 were added separately to Li-IL and mixed by mortar and pestle; then, the resulting mixture was heated at 120°C/12 h to get Li-IL/MOF filler.

Preparation of PEO-LiTFSI/UIO-IL composite electrolyte: membrane of PEO-LiTFSI/UIO-IL solid electrolyte was prepared by the solution casting process. (i) PEO (*M*w = 600,000; Aladdin) and LiTFSI (98% Aladdin) were dissolved into anhydrous acetonitrile with an EO/Li ratio of 18 and stirred at room temperature for 3 h. (ii) Nanostructured UIO/Li-IL fillers were added to the obtained (PEO-LiTFSI) mixture with various ratios (0%, 10%, 20%, 30%, and 40%), and then stirred to get a homogeneous mixture. (iii) The obtained mixture (PEO-LiTFSI/UIO-IL) was poured onto polytetrafluoroethylene molds and stabilized at 25°C for 24 h to evaporate the solvent slowly before drying at 60°C overnight under vacuum to get the PEO-LiTFSI/UIO-IL composite electrolyte.

Preparation of the cathode: commercial $LiFePO_4$ (Shenzhen Dynanonic Co., Ltd), acetylene black, and UIO-66@67-IL with a ratio of 5:2:5 were dissolved in an appropriate volume of *N*-methyl-2-pyrrolidone with a magnetic stirrer overnight at room temperature to obtain a homogenous solution. The resulting mixture was cast over aluminum foil before being heated at 120°C for 12 h. The weight of the active material in the cathode is 4 mg cm^{-2}.

Materials characterization

Field emission scanning electron microscopy (SEM) images of UIO-66, 67, 66@67, and PEO-LiTFSI/UIO-IL samples were collected by a JEOL 7100F microscope with an acceleration voltage of 20 kV. An Oxford IE250 system was used to generate energy-dispersive X-ray spectra (EDS). Transmission electron microscopy (TEM) images were collected using a JEM-2100 TEM microscope with a 200 kV acceleration voltage. The crystallographic characterization was conducted using a BRUKER 2ndGen diffractometer with a Cu tube radiation and 2θ from 5° to 40°. Raman spectra were collected with a Renishaw RM-1000 Raman microscopy system. The Brunauer–Emmett–Teller (BET) specific surface area was determined by using a Micromeritics ASAP 2020 instrument at 77 K. Fourier transform infrared (FTIR) spectroscopy analyses were done *via* a Nicolet 6700 IR spectrometer with the wave range of 400–4000 cm^{-1}. Differential scanning calorimetry (DSC) was conducted from −50 to 90°C under Ar atmosphere using a DSC Q2000 simultaneous analyzer. Netzsch STA 449C simultaneous analyzer was used for the thermogravimetric analysis (TGA) from 30 to 700°C

with a heating rate of 10°C min^{-1} in argon atmosphere.

Electrochemical measurements

The ionic conductivity of stainless steel/PEO-LiTFSI/UIO-IL/stainless steel was measured using electrochemical impedance spectroscopy (EIS) with a frequency range from 0.1 to 10^6 Hz by Auto-Lab PGSTAT302N. The activation energy (E_a) was determined by measuring the ionic conductivity at various temperatures and calculated based on the Arrhenius equation. t_{Li^+} of Li/PEO-LiTFSI/UIO-IL/Li has been measured by a combination of alternating current (AC) impedance and direct current (DC) polarization measurements using A NOVOCONTROL spectrometer system with a DC potential of 10 mV. The electrochemical stability (ESW) of stainless steel/PEO-LiTFSI/UIO-IL/Li was measured by linear sweep voltammetry (LSV) using a NOVOCONTROL spectrometer workstation from 0 to 6 V with a scan rate of 5 mV s^{-1}. The galvanostatic cycling (Li plating/stripping) of PEO-LiTFSI/UIO-IL solid electrolyte against lithium metal anodes was investigated by a Li symmetrical cell using the multichannel battery testing system LANHE CT2001A. Cathode mixture, PEO-LiTFSI/UIO-IL solid electrolyte, and lithium metal anode were assembled into the CR2016 cell to measure the cycle performance and rate capacity.

RESULTS AND DISCUSSION

Two steps were used to construct UIO-66@67 spherical nanoparticles with heterogeneous pore structures. In brief, Zr forms a bond with the first ligand H_2-BDC to form the core structure (UIO-66), which is followed by the second ligand H_2-BPDC, which forms the shell framework (UIO-67). The presence of the UIO-66@67 core-shell structure was determined using X-ray diffraction (XRD), FTIR, SEM, and TEM characterizations. Comparative XRD analysis in Fig. S1a (Supplementary information) suggests that XRD patterns of pure MOFs (UIO-66 and UIO-67) are possessed in the patterns of UIO-66@67. In addition, FTIR analysis (Fig. S1b) confirms the presence of coordination between metal sets and linkers in the MOF structure *via* the bridges. This is attributed to the linker deprotonation, which is verified by the evanescence of the OH^- stretching vibrations from the organic ligands between 2500 and 3000 cm^{-1}. Moreover, compared with the vibration of original linkers, a significant shift in stretching vibration of C=O at 1680 cm^{-1} in the MOFs is detected. Based on differences in shape and contrast, SEM and TEM characterizations were also used to confirm the morphology of the UIO-66@67 core-shell. Pure MOFs UIO-66 and UIO-67 have cubic and octahedron shapes, respectively, with particle sizes of around 100 nm, as shown in Fig. S1c, d, whereas the morphology of UIO-66@67 is spherical nanoparticles (Fig. S1e). Furthermore, the contrast between the shell and core structure differentiates UIO-67 growth on the surface of UIO-66 (Fig. S1f). Based on the above results, we successfully prepared UIO-66@67 nanoparticles with a size around 140 nm.

As shown in Fig. S1g, UIO-66@67 has a high specific surface area (2000 m^2 g^{-1}), which increases the dissolution amount of Li-IL. Furthermore, depending on the confinement of $[TFSI]^-$ and $[EMIM]^+$ by core structure nanopores due to the equality between the sizes of the $[TFSI]^-$ and $[EMIM]^+$ ions (7.9 and 7.6 Å, respectively) [42], the Li^+ is free in UIO-66@67-IL fillers as illustrated by FTIR (Fig. S1h). Therefore, we successfully obtained UIO-66@67-IL fillers with high ionic conductivity reaching 2.1 × 10^{-3} S cm^{-1} at 27°C (Fig. S1i).

The mechanism of BBLN solid polymer electrolyte formation is illustrated in Fig. 1a. Surprisingly, the SEM image (Fig. 1b) shows that the surface of BBLN solid polymer electrolyte has a significant number of convolutions with average diameters (150 nm) that are similar to the cerebral cortex convolutions in the brain (Fig. 1c). As a result, when compared with the sharp edge of UIO-66 and UIO-67 (cubic and octahedral) fillers Fig. S1c, d, UIO-66@67 spherical nanoparticles (Fig. S1e, f) are highly appealing to minimize stress and deformation of polymer electrolytes. As shown in Fig. S2, the polymer solution casting technique was successfully used to produce stable and flexible BBLN solid polymer electrolytes. Cross-section SEM images of BBLN solid polymer electrolyte at various magnifications revealed continuous convolutions, similar to those found in the brain, throughout the electrolyte (Fig. S3a, b). The polymer electrolyte in Fig. S3c–f has a highly uniform distribution of Zr, S, F, and C elements, indicating that the UIO-66@67-IL fillers are uniformly distributed in the polymer electrolyte matrix.

Thermal property is a key parameter to guarantee the safe operation of lithium batteries at various temperatures. We used TGA to determine the thermal stability of BBLN solid polymer electrolytes. The plots of UIO-66@67 nanoparticles, UIO-66@67-IL fillers, PEO-LiTFSI, and BBLN solid polymer electrolyte film are shown in Fig. S4. PEO-LiTFSI breakdown begins at 360°C, whereas BBLN solid polymer electrolyte decomposition occurs at 420°C. This effect is caused by the incorporation of UIO-66@67 spherical nanoparticles, which have high thermal stability of up to 560°C. These findings also imply that UIO-66@67 can reduce polymer/LiTFSI crystallinity. Based on the foregoing, BBLN solid polymer electrolytes can be used in solid-state LIBs without risk.

The ionic conductivity of the solid electrolyte is a crucial parameter for its practical application in solid-state batteries. Arrhenius plots of solid polymer electrolytes with varying compositions were investigated to control the amount of incorporated UIO-66@67-IL fillers that result in higher ionic conductivity. Fig. S5a shows that the PEO-LiTFSI solid electrolyte has a low ionic conductivity of 5.5 × 10^{-6} S cm^{-1}, owing to polymer crystalline domains that restrict the mobility of the ions. On the other hand, the ionic conductivity of BBLN solid polymer electrolyte gradually increased by increasing the

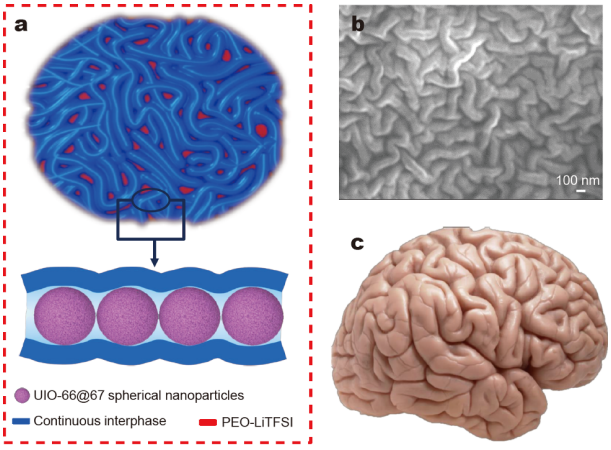

Figure 1 (a) Schematic diagram of the architecture design of BBLNs. (b) SEM image of BBLN solid polymer electrolyte. (c) Schematic of brain structure.

amount of UIO-66@67-IL fillers, and reached 9.2 × 10^{-4} S cm^{-1} at 40% UIO-66@67-IL fillers. Based on the ionic conductivity, stretchability, and visual appearance, we decided to use an electrolyte containing 40% UIO-66@67-IL fillers. Fig. S5b depicts the relationship between the ionic conductivities and temperature of a BBLN solid polymer electrolyte containing 40% UIO-66@67-IL from −20 to 100°C. As can be seen, the conductivity increases with the temperature. This is due to the improved interface between UIO-66@67 spherical nanoparticles and polymer electrolyte after heating, which provides an early indication of the stability of BBLN solid polymer electrolyte at high and low temperatures. Moreover, the BBLN solid polymer electrolyte with different concentrations presents higher ionic conductivity at the same temperature than PEO-LiTFSI solid electrolyte, as displayed in Fig. S5c. This phenomenon can be attributed to the following factors: UIO-66@67 spherical nanoparticles provide a significant number of continuous convolutions by reducing polymer electrolyte deformation, resulting in a highly conductive pathway along the polymer/UIO-66@67 interphase. Besides, UIO-66@67 spherical nanoparticles with a high surface area can dramatically reduce the crystallinity and enhance the segmental movement of polymer-LiTFSI (Fig. S6), raising the ionic conductivity. Moreover, the uniform distribution of highly conducive UIO-66@67 fillers in polymer electrolytes results in fast and optimal ion transport pathways.

Further characterization indicates the BBLN solid polymer electrolyte is typically constituted of linked labyrinthine networks with diameters ranging from 140 to 160 nm (Fig. S7a), while the morphologies of polymer-LiTFSI/UIO-66-IL and polymer-LiTFSI/UIO-67-IL consist of spotted structures (Fig. S7b, c). The BBLN solid polymer electrolyte improves the ionic conductivity compared with polymer-LiTFSI/UIO-66-IL (1 × 10^{-4} S cm^{-1}), polymer-LiTFSI/UIO-67-IL (1.9 × 10^{-4} S cm^{-1}), and recent studies as shown in Fig. 2a, b, c, Table S1, and other phase separation studies [43–46].

PEO-LiTFSI/UIO-66-IL, PEO-LiTFSI/UIO-67-IL, and BBLN solid polymer electrolytes were subjected to LSV experiments at 25°C to investigate the electrochemical stability window of

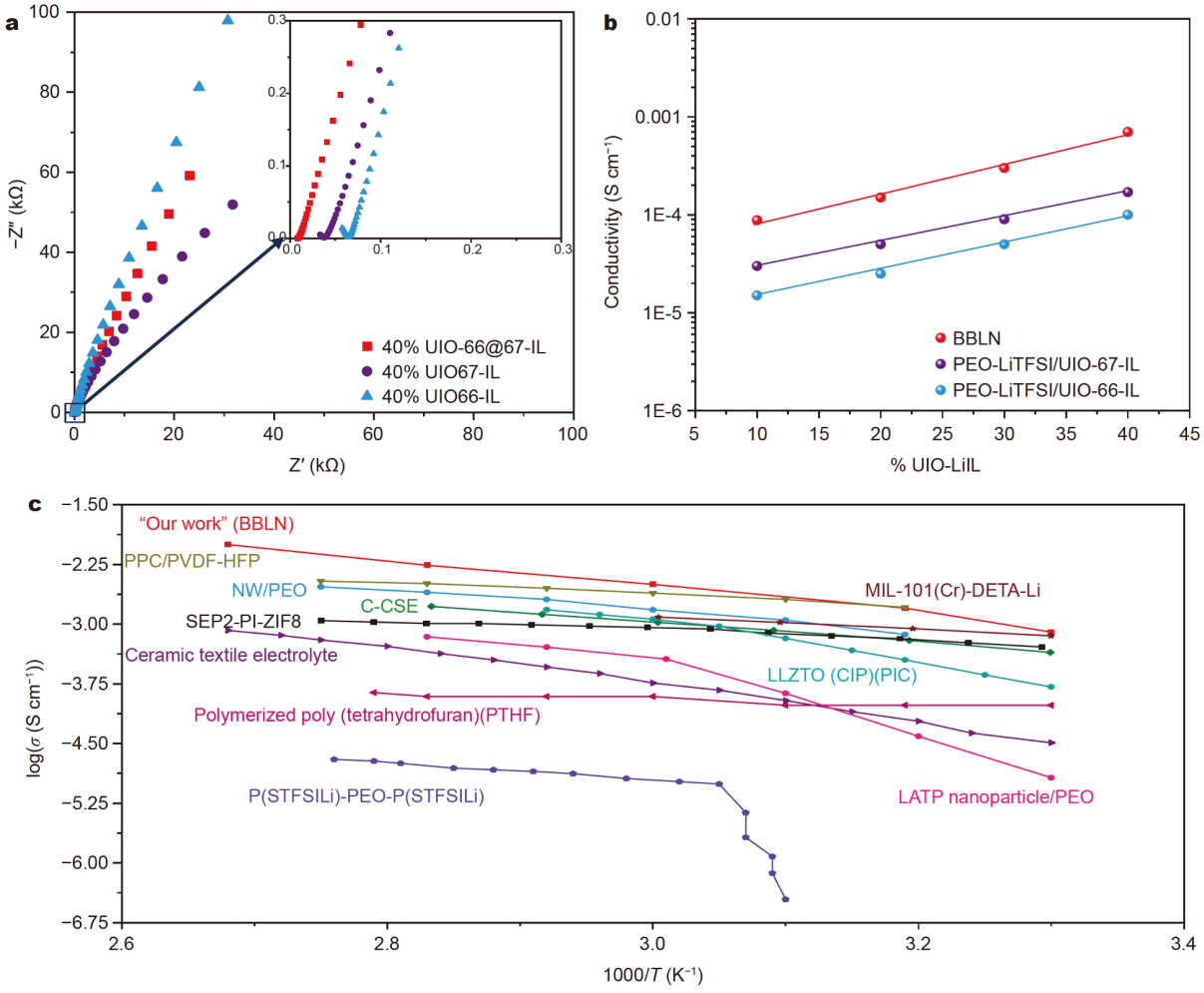

Figure 2 Electrochemical characterization of solid electrolyte. (a) Comparison among AC impedance spectra of BBLN, PEO-LiTFSI/UIO-66-IL, PEO-LiTFSI/UIO-67-IL solid electrolytes at room temperature. (b) Arrhenius plots of BBLN solid polymer electrolyte, PEO-LiTFSI/UIO-66-IL, PEO-LiTFSI/UIO-67-IL solid electrolyte with different compositions at room temperature. (c) Comparison of Arrhenius plots of BBLN solid polymer electrolyte (red) with other reported electrolytes such as cross-linked composite solid electrolyte (C-CSE) [47], P(STFSILi)-PEO-P(STFSILi) [48], MIL-101(Cr)-DETA-Li [49], SEP-PI-ZIF8 [50], supper ionic conductor hierarchical poly(ionic liquid)-based solid electrolyte (HPILSE) [51], gel blending polymer electrolyte PPC/PVDF-HFP [poly(vinylidenefluoride-hexafluoropropylene)-poly(propylene carbonate)] [52], P(STFSILi)-PEO-P(STFSILi) [53], ceramic textile electrolyte $Li_7La_3Zr_2O_{12}$ [54], $Li_7La_3Zr_2O_{12}$ nanowire-PEO [55], LATP nanoparticle/PEO [56], and LLZTO (CIP)(PIC) electrolytes [57].

electrolytes. As displayed in Fig. S8a–c, the stable voltage windows of PEO-LiTFSI/UIO-66-IL and PEO-LiTFSI/UIO-67-IL are 1.2–4.5 V and 1.8–5.5 V, respectively, which are narrower than that of BBLN solid polymer electrolyte (0.0–5.5 V). Compared with PEO-LiTFSI/UIO-66-IL and PEO-LiTFSI/UIO-67-IL, BBLNs have higher stability against cathodic reduction and anodic oxidation reactions. This result can be attributed to BBLNs' high surface area, which can improve impurity absorption from the electrode/electrolyte interface, as well as the high interaction between UIO-66@67-IL and polymer-LiTFSI. As a result, the electrochemical stability window of BBLN solid polymer electrolytes is appropriate for application in LIBs.

The lithium-ion transference number (t_{Li}^+) of solid electrolytes needs to be high enough because it can prophesy the formation of lithium dendrites. A high lithium-ion transference number is necessary for solid electrolytes because the moving of anions highly affects Li^+ polarization during the charging and discharging processes. t_{Li}^+ was calculated by the DC polarization curve at 25°C. BBLN solid polymer electrolyte exhibits a high t_{Li}^+ of 0.74, as shown in Fig. 3a. This result is higher than that of polymer-LiTFSI/UIO-66-IL (t_{Li}^+ = 0.37) and also much higher than that of polymer-LiTFSI/UIO-67-IL (t_{Li}^+= 0.25) as illustrated in Fig. 3c, e, respectively. The high lithium-ion transference number of BBLN solid polymer electrolyte can be attributed to the large number of highly uniform continuous convolutions of BBLNs, resulting in a highly conductive pathway along the polymer/UIO-66@67 interphase (Fig. 3b), as opposed to polymer-LiTFSI/UIO-66-IL (Fig. 3d) and polymer-LiTFSI/UIO-67-IL (Fig. 3f). Besides, the repression of the free movement of ionic liquid ions ($TFSI^-$) by UIO-66@67 pore channels leads to the splitting of the lithium salt ion pairs and increases the content of Li^+. The dissociation degree of the lithium salt in BBLN solid polymer electrolyte and polymer-LiTFSI electrolyte was investigated using Raman spectra. As a result, the dissociation degree of Li salt in BBLN solid polymer electrolyte is 85.8%, which is higher than that in polymer-LiTFSI (65%), as shown in Fig. S9 [58]. Moreover, the confinement of ionic liquid ions by incorporated UIO-66@67-IL fillers constructs solid-liquid interphase

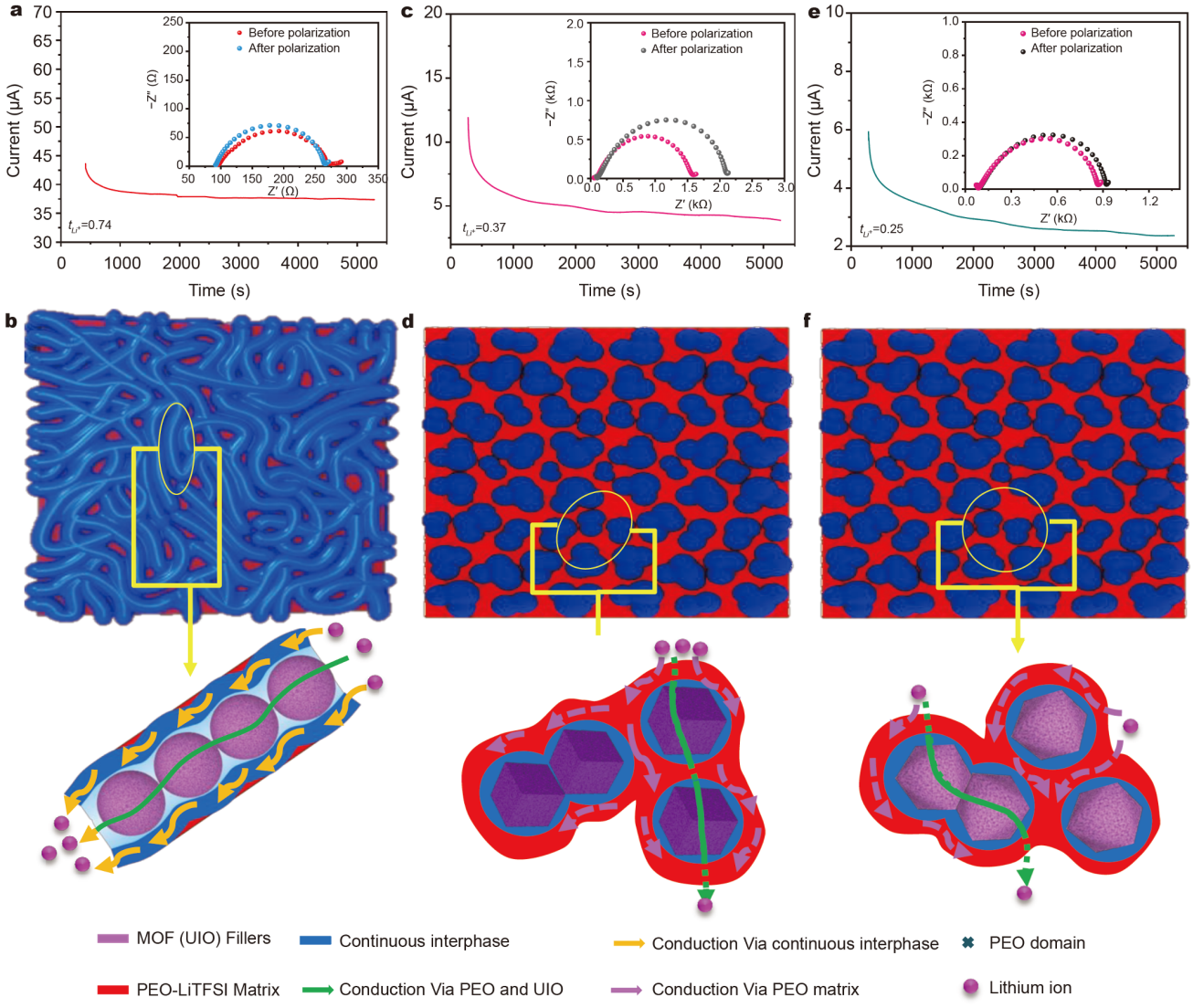

Figure 3 (a, c, e) DC polarization curve of BBLN solid polymer electrolyte, PEO-LiTFSI/UIO-66-IL, and PEO-LiTFSI/UIO-67-IL, respectively, at room temperature. (b, d, f) Schematic illustrating the transport of lithium ions with (b) BBLN solid polymer electrolyte, (d) PEO-LiTFSI/UIO-66-IL solid electrolyte, and (f) PEO-LiTFSI/UIO-67-IL solid polymer electrolytes.

between UIO-66@67-IL and polymer chains. These findings imply that the high lithium-ion transference number of BBLN solid polymer electrolytes could be beneficial for Li^+ deposition by inhibiting the growth of lithium dendrites and reducing the interfacial resistance with lithium electrodes.

The behavior of an electrolyte's Li plating and stripping is a critical parameter in determining the lifetime of Li batteries, especially when long-term cycling is anticipated. These experiments were carried out in Li symmetric cells with BBLN solid polymer electrolytes. The Li/BBLN/Li cell was charged and discharged with various current densities (200, 400, and 600 μA cm^{-2}) at 25°C. As shown in Fig. 4a, the BBLN solid polymer electrolyte exhibited excellent stability for over 750 h and low polarization of 0.0192, 0.0468, and 0.0682 V, respectively. Another experiment with BBLN solid polymer electrolyte in symmetric Li/Li batteries was carried out for further investigation at a current density of 400 μA cm^{-2}. As shown in Fig. 4b, the BBLN solid polymer electrolyte maintains low voltage polarization 0.0383 V with excellent stability over 6500 h at 25°C. Subsequently, the comparative experiment among BBLN solid polymer electrolyte, polymer-LiTFSI/UIO-66-IL, and polymer-LiTFSI/UIO- 67-IL was implemented at a current density of 200 μA cm^{-2}. Solid polymer electrolytes containing UIO-67-IL and UIO-66-IL show a short circuit after 730 and 650 h, respectively, as shown in Fig. 4c.

Non-uniform deposit of Li^+ on the surface of Li anode in the cells with polymer-LiTFSI/UIO-66-IL and polymer-LiTFSI/UIO-67-IL (Fig. 4d, e) compared with BBLN solid polymer electrolyte (Fig. 4f) leads to the growth of Li dendrites penetrating the electrolyte. This refers to the lack of mechanical strength, which is insufficient to prevent the formation of lithium dendrites. Moreover, spherical nanoparticles with a smooth UIO-66@67 edge, as opposed to sharp edges of other structures (cubic, octahedral, etc.), can protect the electrolyte surface from deformation during lithium plating/stripping. By contrast, the BBLN solid polymer electrolyte showed a very low polarization of 0.02 V with a smooth plateau for more than 1150 cycles without a short circuit. Fig. 4f shows the excellent stability of BBLN solid polymer electrolyte compared with polymer-LiTFSI/UIO-66-IL and polymer-LiTFSI/UIO-67-IL. Furthermore, the lithium anode remained shiny after the operation, with no obvious dendritic structure, indicating that BBLN solid polymer electrolyte effectively inhibits lithium dendrite growth when compared with polymer-LiTFSI/UIO-66-IL and polymer-LiTFSI/UIO-67-IL. In addition, the calculated resistance based on Ohm's law approximately equals 130 Ω cm^{-2}, which is in good agreement with the AC impedance of CSIL solid electrolyte before and after cycling at 200 μA cm^{-2} (Fig. S10). The above results confirm that the BBLN solid polymer electrolyte effectively enhances the transport of Li^+ and evenly distributes the Li^+

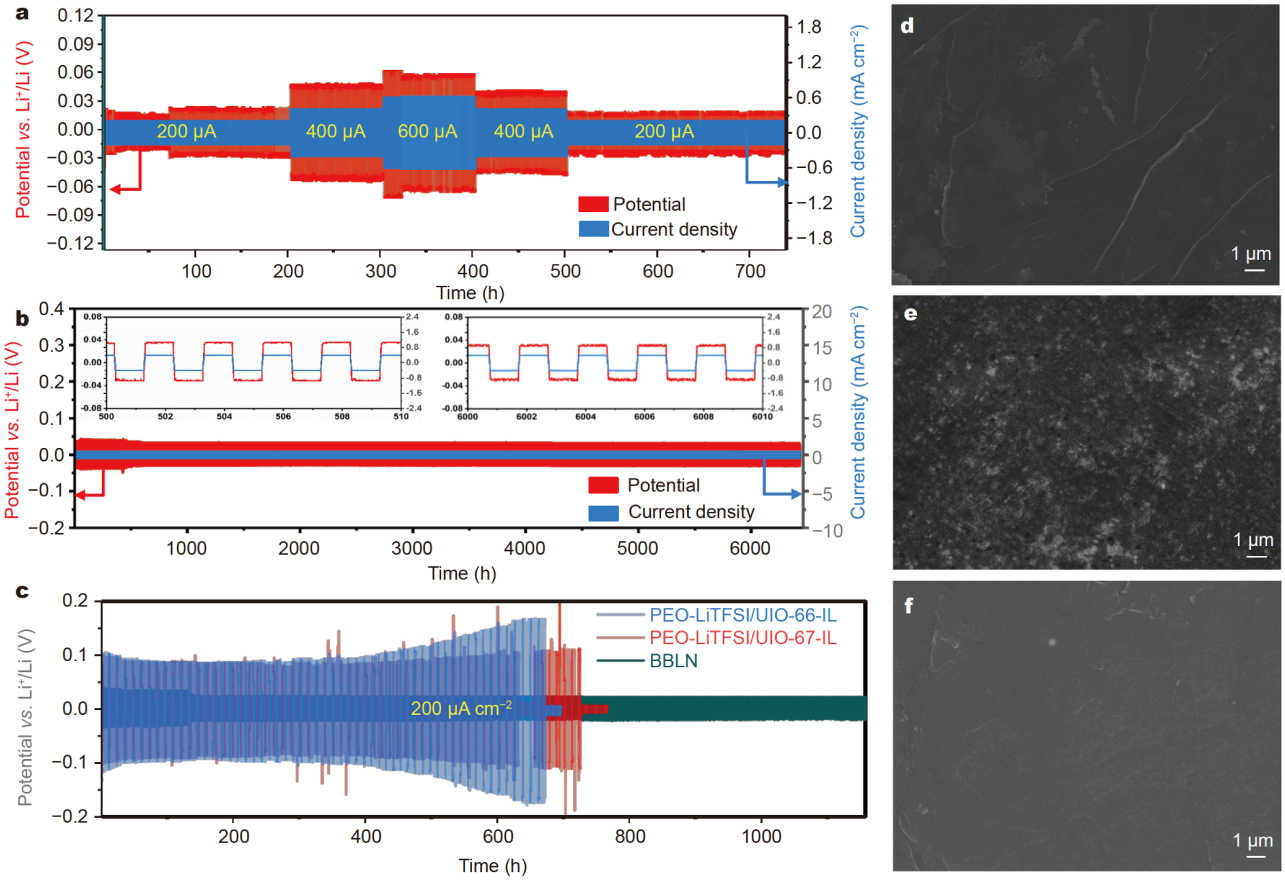

Figure 4 Lithium compatibility cycling of lithium/solid electrolyte/lithium symmetrical cells. (a) Galvanostatic cycling of BBLN solid polymer electrolyte solid electrolyte at different current densities (200, 400, and 600 μA cm^{-2}). (b) Galvanostatic cycling of BBLN solid polymer electrolyte at a current density of 400 μA cm^{-2} at room temperature. (c) Comparison for voltage profiles of BBLN solid polymer electrolyte, PEO-LiTFSI/UIO-66-IL and PEO-LiTFSI/UIO-67-IL at 200 μA cm^{-2} at room temperature. SEM images of Li metal in (d) PEO-LiTFSI/UIO-66-IL, (e) PEO-LiTFSI/UIO-67-IL, and (f) BBLN solid polymer electrolyte.

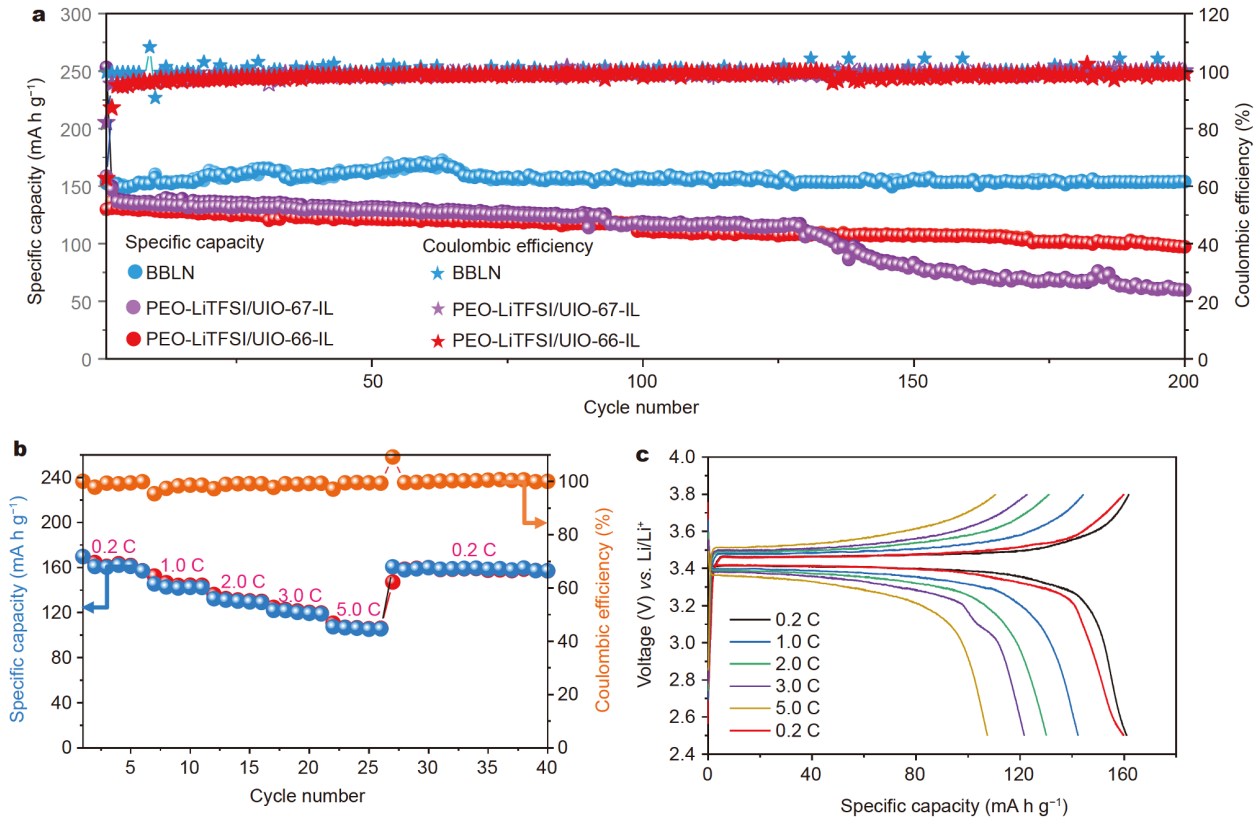

Figure 5 Electrochemical performances of solid-sate batteries. (a) Cycling performance of solid-state batteries with BBLN solid polymer electrolyte, PEO-LiTFSI/UIO-66-IL and PEO-LiTFSI/UIO-67-IL at 0.2 C. (b) Rate performance of solid-state batteries with BBLN solid polymer electrolyte under different charge/discharge rates. (c) Charge/discharge profiles of solid-state batteries with BBLN solid polymer electrolyte at different charge/discharge rates. All tests were conducted at room temperature.

on the Li metal.

Furthermore, to check the utility of BBLN solid polymer electrolytes, the electrochemical performance test was conducted with Li metal as anode and $LiFePO_4$ (LFP) as a cathode. As depicted in Fig. 5a, the LFP/BBLN solid polymer electrolyte/Li batteries at 0.2 C rate showed a high specific capacity of 155 mA h g^{-1}, excellent long-term cycling stability over 200 cycles with capacity retention of 99%. This result is much higher than LFP/polymer-LiTFSI/UIO-66-IL/Li (130.2 mA h g^{-1} with retention of 78.6%) and LFP/polymer-LiTFSI/UIO-67-IL/Li (135.4 mA h g^{-1} with retention of 43.5%). Also, from Fig. 5a, we observed that the capacity of polymer-LiTFSI/UIO-66-IL and polymer-LiTFSI/UIO-67-IL decreased gradually during cycling. When compared with BBLN solid polymer electrolyte, these results can be attributed to low ionic conductivity, low Li-ion transport, high interfacial resistance, and low stability against electrodes.

As shown in Fig. S11a, b, the lithium metal anode contacting the BBLN solid polymer electrolyte after cycling remains shiny with no dendritic structure, indicating that the BBLN solid polymer electrolyte effectively inhibits the formation of Li dendrites. Additionally, the BBLN solid polymer electrolyte after cycling remained intact as the original electrolyte, and no obvious Li dendrites were observed (Fig. S11c, d). The LFP cathode after charge/discharge cycling is more homogeneous than the cathode before cycling, implying that the interface between the BBLN solid polymer electrolyte and the LFP electrode will improve with cycling (Fig. S11e, f). Based on the findings, BBLN solid polymer electrolyte has much better cycling stability and effectively inhibits the growth of lithium dendrites than other recent studies using MOF solid polymer electrolytes (Table S2). This is attributed to the high mechanical strength of the UIO-66@67 spherical nanoparticles, and the homogeneous deposition of lithium on the electrode surface. Furthermore, when compared with the sharp edge particles in UIO-66, UIO-67, and previous works, the smooth edge of UIO-66@67 spherical nanoparticles can protect the surface of BBLNs from distortion caused by the stress of lithium electrode expansion and shrinkage during cycling.

The capacity of cathodes with BBLN solid polymer electrolyte at various rates ranging from 0.2 C to 5 C is depicted in Fig. 5b, c. The cathodes present an excellent specific charge and discharge capacity of 161, 145, 133, 124, 110, and 160 mA h g^{-1}, respectively. Furthermore, the batteries at 0.2 C exhibit a flat potential plateau during charging and discharging cycles at 3.48 and 3.40 V. This means that the batteries maintain a low polarization of 0.08 V while cycling. It is worth noting that when the rate was reversed back to 0.2 C, the specific capacity of Li batteries almost recovered (160 mA h g^{-1}), indicating that LFP/BBLN/Li batteries have excellent stability. We also carried out a cycling test at 3 C to explore the cycling stability and lifetime of LFP/BBLN/Li batteries at high current density, as shown in Fig. S12. After 700 cycles, we found that 88.42% of the initial capacity was retained, indicating that the BBLN solid polymer electrolyte effectively functions as a Li-ion conductor for solid-state LIBs. Overall, the novel BBLN solid polymer electrolyte

appears to be a promising candidate for room-temperature solid-state LIBs.

CONCLUSIONS

In conclusion, we successfully designed and fabricated an interesting BBLN solid polymer electrolyte using integrated spherical nanoparticles. The proposed solid polymer electrolyte has the potential to significantly reduce the interfacial resistance between the electrode and the electrolyte. Meanwhile, it inhibits the formation of lithium dendrites. Besides, BBLN solid polymer electrolyte improves Li^+ transport and maintains a uniform deposition of Li^+ on the surface of the Li electrode. Benefiting from these merits, BBLN solid polymer electrolyte exhibits an excellent ionic conductivity of 9.2×10^{-4} S cm^{-1}, high t_{Li^+} of 0.74 at 25°C, and superior stability against lithium metal over 6500 h at 400 μA cm^{-2}. Furthermore, after 200 cycles at 0.2 C, room temperature, integrated solid-state LIBs based on BBLN solid polymer electrolytes demonstrated an excellent capacity of 155 mA h g^{-1}. Finally, our designed electrolyte opens up a new avenue for using brain-like nanostructures for solid polymer electrolytes to improve electrochemical performance.

Received 2 November 2021; accepted 17 December 2021; published online 18 February 2022

1 Chheda JN, Huber GW, Dumesic JA. Liquid-phase catalytic processing of biomass-derived oxygenated hydrocarbons to fuels and chemicals. Angew Chem Int Ed, 2007, 46: 7164–7183
2 Yu D, Wu B, Ge L, *et al.* Decorating nanoporous ZIF-67-derived $NiCo_2O_4$ shells on a Co_3O_4 nanowire array core for battery-type electrodes with enhanced energy storage performance. J Mater Chem A, 2016, 4: 10878–10884
3 Guan BY, Yu L, Wang X, *et al.* Formation of onion-like $NiCo_2S_4$ particles *via* sequential ion-exchange for hybrid supercapacitors. Adv Mater, 2017, 29: 1605051
4 Li S, Zhang SQ, Shen L, *et al.* Progress and perspective of ceramic/polymer composite solid electrolytes for lithium batteries. Adv Sci, 2020, 7: 1903088
5 Sun J, Yao X, Li Y, *et al.* Facilitating interfacial stability *via* bilayer heterostructure solid electrolyte toward high-energy, safe and adaptable lithium batteries. Adv Energy Mater, 2020, 10: 2000709
6 Zhang D, Xu X, Qin Y, *et al.* Recent progress in organic–inorganic composite solid electrolytes for all-solid-state lithium batteries. Chem Eur J, 2020, 26: 1720–1736
7 Zhang J, Li L, Zheng C, *et al.* Silicon-doped argyrodite solid electrolyte Li_6PS_5I with improved ionic conductivity and interfacial compatibility for high-performance all-solid-state lithium batteries. ACS Appl Mater Interfaces, 2020, 12: 41538–41545
8 Yu S, Schmohl S, Liu Z, *et al.* Insights into a layered hybrid solid electrolyte and its application in long lifespan high-voltage all-solid-state lithium batteries. J Mater Chem A, 2019, 7: 3882–3894
9 Zhang X, Wang S, Xue C, *et al.* Self-suppression of lithium dendrite in all-solid-state lithium metal batteries with poly(vinylidene difluoride)-based solid electrolytes. Adv Mater, 2019, 31: 1806082
10 Gao Z, Sun H, Fu L, *et al.* Promises, challenges, and recent progress of inorganic solid-state electrolytes for all-solid-state lithium batteries. Adv Mater, 2018, 30: 1705702
11 Zhang Z, Shao Y, Lotsch B, *et al.* New horizons for inorganic solid state ion conductors. Energy Environ Sci, 2018, 11: 1945–1976
12 Bachman JC, Muy S, Grimaud A, *et al.* Inorganic solid-state electrolytes for lithium batteries: mechanisms and properties governing ion conduction. Chem Rev, 2016, 116: 140–162
13 Janek J, Zeier WG. A solid future for battery development. Nat Energy, 2016, 1: 1–4
14 Dirican M, Yan C, Zhu P, *et al.* Composite solid electrolytes for all-solid-state lithium batteries. Mater Sci Eng-R-Rep, 2019, 136: 27–46
15 Zhou X, Jiang H, Zheng H, *et al.* Nonflammable hybrid solid electrolyte membrane for a solid-state lithium battery compatible with conventional porous electrodes. J Membrane Sci, 2020, 603: 117820
16 Homann G, Stolz L, Winter M, *et al.* Elimination of "Voltage noise" of poly (ethylene oxide)-based solid electrolytes in high-voltage lithium batteries: linear *versus* network polymers. iScience, 2020, 23: 101225
17 Zheng F, Kotobuki M, Song S, *et al.* Review on solid electrolytes for all-solid-state lithium-ion batteries. J Power Sources, 2018, 389: 198–213
18 Zhang Q, Liu K, Ding F, *et al.* Recent advances in solid polymer electrolytes for lithium batteries. Nano Res, 2017, 10: 4139–4174
19 Zhou D, He YB, Liu R, *et al. In situ* synthesis of a hierarchical all-solid-state electrolyte based on nitrile materials for high-performance lithium-ion batteries. Adv Energy Mater, 2015, 5: 1500353
20 Xu L, Tang S, Cheng Y, *et al.* Interfaces in solid-state lithium batteries. Joule, 2018, 2: 1991–2015
21 Lv F, Wang Z, Shi L, *et al.* Challenges and development of composite solid-state electrolytes for high-performance lithium ion batteries. J Power Sources, 2019, 441: 227175
22 Xue Z, He D, Xie X. Poly(ethylene oxide)-based electrolytes for lithium-ion batteries. J Mater Chem A, 2015, 3: 19218–19253
23 Zhao R, Liang Z, Zou R, *et al.* Metal-organic frameworks for batteries. Joule, 2018, 2: 2235–2259
24 Chen N, Li Y, Dai Y, *et al.* A Li^+ conductive metal organic framework electrolyte boosts the high-temperature performance of dendrite-free lithium batteries. J Mater Chem A, 2019, 7: 9530–9536
25 Abdelmaoula AE, Shu J, Cheng Y, *et al.* Core–shell MOF-in-MOF nanopore bifunctional host of electrolyte for high-performance solid-state lithium batteries. Small Methods, 2021, 5: 2100508
26 Wang Z, Wang Z, Yang L, *et al.* Boosting interfacial Li^+ transport with a MOF-based ionic conductor for solid-state batteries. Nano Energy, 2018, 49: 580–587
27 Wu JF, Guo X. Nanostructured metal–organic framework (MOF)-derived solid electrolytes realizing fast lithium ion transportation kinetics in solid-state batteries. Small, 2019, 15: 1804413
28 Adrian PN, Andreas O, Dan C. Numerical analysis of the diffusive mass transport in brain tissues with applications to optical sensors. Proc of SPIE, 2013, 8576: 857605
29 Silbernagel S, Despopoulos A. Taschenatlas Physiologie. New York: Thieme Stuttgart, 2012
30 Jiang J, Guo J, Wan X, *et al.* 2D MoS_2 neuromorphic devices for brain-like computational systems. Small, 2017, 13: 1700933
31 Nicholson C. Diffusion and related transport mechanisms in brain tissue. Rep Prog Phys, 2001, 64: 815–884
32 Tauseefur R, Eldad H, Kilian MP, *et al.* Multimodal registration of white matter brain data *via* optimal mass transport. Midas J, 2008, 27–35
33 Gallos LK, Makse HA, Sigman M. A small world of weak ties provides optimal global integration of self-similar modules in functional brain networks. Proc Natl Acad Sci USA, 2012, 109: 2825–2830
34 Ma M, Wang X, Duan Y, *et al.* Optimal mass transport based brain morphometry for patients with congenital hand deformities. Vis Comput, 2019, 35: 1311–1325
35 Chen Y, Wang Q, Wang T. Facile large-scale synthesis of brain-like mesoporous silica nanocomposites *via* a selective etching process. Nanoscale, 2015, 7: 16442–16450
36 Ray LA, Heys JJ. Fluid flow and mass transport in brain tissue. Fluids, 2019, 4: 196
37 Agaliotis EM, Rosenberger MR, Ares AE, *et al.* Influence of the shape of the particles in the solidification of composite materials. Procedia Mater Sci, 2012, 1: 58–63
38 Zhu Y, Li J, Wan M, *et al.* A new route for the preparation of brain-like nanostructured polyaniline. Macromol Rapid Commun, 2007, 28: 1339–1344
39 Seo S-, Park D, Park S, *et al.* "Brain-coral-like" mesoporous hollow CoS_2@N-doped graphitic carbon nanoshells as efficient sulfur reservoirs for lithium–sulfur batteries. Adv Funct Mater, 2019, 29: 1903712
40 Zhou JJ, Wang R, Liu XL, *et al. In situ* growth of CDS nanoparticles on

Uio-66 metal-organic framework octahedrons for enhanced photocatalytic hydrogen production under visible light irradiation. Appl Surf Sci, 2015, 346: 278–283
41 Øien-Ødegaard S, Bouchevreau B, Hylland K, *et al.* UiO-67-type metal–organic frameworks with enhanced water stability and methane adsorption capacity. Inorg Chem, 2016, 55: 1986–1991
42 Largeot C, Portet C, Chmiola J, *et al.* Relation between the ion size and pore size for an electric double-layer capacitor. J Am Chem Soc, 2008, 130: 2730–2731
43 Wang Z, Wang S, Wang A, *et al.* Covalently linked metal–organic framework (MOF)-polymer all-solid-state electrolyte membranes for room temperature high performance lithium batteries. J Mater Chem A, 2018, 6: 17227–17234
44 Porcarelli L, Gerbaldi C, Bella F, *et al.* Super soft all-ethylene oxide polymer electrolyte for safe all-solid lithium batteries. Sci Rep, 2016, 6: 19892
45 Schulze MW, McIntosh LD, Hillmyer MA, *et al.* High-modulus, high-conductivity nanostructured polymer electrolyte membranes *via* polymerization-induced phase separation. Nano Lett, 2014, 14: 122–126
46 Chopade SA, Au JG, Li Z, *et al.* Robust polymer electrolyte membranes with high ambient-temperature lithium-ion conductivity *via* polymerization-induced microphase separation. ACS Appl Mater Interfaces, 2017, 9: 14561–14565
47 Xia Y, Xu N, Du L, *et al.* Rational design of ion transport paths at the interface of metal–organic framework modified solid electrolyte. ACS Appl Mater Interfaces, 2020, 12: 22930–22938
48 Bouchet R, Maria S, Meziane R, *et al.* Single-ion BAB triblock copolymers as highly efficient electrolytes for lithium-metal batteries. Nat Mater, 2013, 12: 452–457
49 Li D, Wang J, Guo S, *et al.* Molecular-scale interface engineering of metal–organic frameworks toward ion transport enables high-performance solid lithium metal battery. Adv Funct Mater, 2020, 30: 2003945
50 Wang G, He P, Fan LZ. Asymmetric polymer electrolyte constructed by metal–organic framework for solid-state, dendrite-free lithium metal battery. Adv Funct Mater, 2020, 31: 2007198
51 Zhou D, Liu R, Zhang J, *et al. In situ* synthesis of hierarchical poly(ionic liquid)-based solid electrolytes for high-safety lithium-ion and sodium-ion batteries. Nano Energy, 2017, 33: 45–54
52 Liang YF, Xia Y, Zhang SZ, *et al.* A preeminent gel blending polymer electrolyte of poly(vinylidene fluoride-hexafluoropropylene)-poly(propylene carbonate) for solid-state lithium ion batteries. Electrochim Acta, 2019, 296: 1064–1069
53 Huang S, Cui Z, Qiao L, *et al.* An *in-situ* polymerized solid polymer electrolyte enables excellent interfacial compatibility in lithium batteries. Electrochim Acta, 2019, 299: 820–827
54 Gong Y, Fu K, Xu S, *et al.* Lithium-ion conductive ceramic textile: a new architecture for flexible solid-state lithium metal batteries. Mater Today, 2018, 21: 594–601
55 Wan Z, Lei D, Yang W, *et al.* Low resistance-integrated all-solid-state battery achieved by $Li_7La_3Zr_2O_{12}$ nanowire upgrading polyethylene oxide (PEO) composite electrolyte and PEO cathode binder. Adv Funct Mater, 2019, 29: 1805301
56 Liu L, Chu L, Jiang B, *et al.* $Li_{1.4}Al_{0.4}Ti_{1.6}(PO_4)_3$ nanoparticle-reinforced solid polymer electrolytes for all-solid-state lithium batteries. Solid State Ion, 2019, 331: 89–95
57 Huo H, Chen Y, Luo J, *et al.* Rational design of hierarchical "ceramic-in-polymer" and "polymer-in-ceramic" electrolytes for dendrite-free solid-state batteries. Adv Energy Mater, 2019, 9: 1804004
58 Huo H, Sun J, chen C, *et al.* Flexible interfaces between Si anodes and composite electrolytes consisting of poly(propylene carbonates) and garnets for solid-state batteries. J Power Sources, 2018, 383: 150–156

Acknowledgements This work was supported by the National Natural Science Foundation of China (51802239 and 52127816), the National Key Research and Development Program of China (2020YFA0715000), the Key Research and Development Program of Hubei Province (2021BAA070), Foshan Xianhu Laboratory of the Advanced Energy Science and Technology Guangdong Laboratory (XHT2020-005), and the Fundamental Research Funds for the Central Universities (2020III011GX, 2020IVB057, 2019IVB054 and 2019III062JL).

Author contributions Abdelmaoula AE performed all the experiments and the data analyses as well as wrote the manuscript; Xu L and Mai L were in charge of this scientific research project, and the leaders of actual coordination of contributions; Abdelmaoula AE, Cheng Y, Mahdy AA, Tahir M and Liu Z contributed to the theoretical analysis. All authors contributed to the general discussion.

Conflict of interest The authors declare no conflict of interest.

Supplementary information Supporting data are available in the online version of the paper.

Ahmed Eissa Abdelmaoula is currently pursuing his PhD degree at the School of Material Science and Engineering, Wuhan University of Technology (WUT). His research interests include the design and fabrication of solid electrolyte materials for energy storage.

Lin Xu is a professor of materials science and engineering at the School of Materials Science and Engineering, WUT. He received his PhD degree from WUT in 2013 and worked as a postdoctoral fellow at Harvard University in 2013–2016. His research focuses on the electrochemical energy storage.

Liqiang Mai is a Chair Professor of materials science and engineering at WUT, Dean of the School of Materials Science and Engineering, WUT, Fellow of the Royal Society of Chemistry. He received his PhD from WUT in 2004 and carried out his postdoctoral research at Georgia Institute of Technology in 2006–2007. He worked as an advanced research scholar at Harvard University in 2008–2011 and the University of California, Berkeley in 2017. His current research interests focus on new nanomaterials for electrochemical energy storage and micro/nano energy devices.

仿生脑状纳米结构的固态聚合物电解质实现快速锂离子输运

Ahmed Eissa Abdelmaoula[1,3†], 杜路路[1†], 徐林[1,2*], 程宇[1], Amir A. Mahdy[3], Muhammad Tahir[1], 刘子昂[1], 麦立强[1,2*]

摘要 电解液的固有缺陷以及锂枝晶问题严重限制了当前商业化锂离子电池的发展. 为了解决上述问题, 本文通过控制加入纳米填料的形状, 获得了具有仿生脑状纳米结构的固态聚合物电解质(BBLN). 与传统复合聚合物固态电解质不同, 我们通过添加球状核壳UIO-66@67纳米填料制备了具有仿生脑状纳米结构的固态聚合物电解质. 球状UIO-66@67纳米颗粒能够有效减小聚合物基质在固化过程中的形变, 从而促进形成独特的仿生脑状纳米结构. 此外, 球状纳米颗粒能够有效降低聚合物电解质的结晶度, 提高其链段运动能力, 形成连续的锂离子传输路径. 基于此, 仿生脑状固态聚合物电解质具有高离子电导率(9.2×10^{-4} S cm^{-1}), 高锂离子迁移数(0.74)和良好的锂金属兼容性(>6500 h). 本研究中提出的仿生脑状纳米结构的设计理念是一种有效增强固态电池中聚合物基电解质的离子输运的新策略.

